JACS
JOURNAL OF THE AMERICAN CHEMICAL SOCIETY
Article
pubs.acs.org/JACS

A Mobile Precursor Determines Amyloid-β Peptide Fibril Formation at Interfaces

Lei Shen, Takuji Adachi, David Vanden Bout, and X.-Y. Zhu*

Department of Chemistry and Biochemistry, The University of Texas at Austin, Austin, Texas 78712, United States

Supporting Information

ABSTRACT: The aggregation of peptides into amyloid fibrils plays a crucial role in various neurodegenerative diseases. While it has been generally recognized that fibril formation in vivo may be greatly assisted or accelerated by molecular surfaces, such as cell membranes, little is known about the mechanism of surface-mediated fibrillation. Here we study the role of adsorbed Alzheimer's amyloid-β peptide (Aβ42) on surface-mediated fibrillation using polymer coatings of varying hydrophobicity as well a supported lipid bilayer membrane. Using single molecule fluorescent tracking and atomic force microscopy imaging, we show that weakly adsorbed peptides with two-dimensional diffusivity are critical precursors to fibril growth on surfaces. This growth mechanism is inhibited on the highly hydrophilic surface where the surface coverage of adsorbed peptides is negligible or on the highly hydrophobic surface where the diffusion constant of the majority of adsorbed peptides is too low. Physical properties that favor weakly adsorbed peptides with sufficient translational mobility can locally concentrate peptide molecules on the surface and promote inter-peptide interaction via two-dimensional confinement, leading to fibrillation at Aβ peptide concentration many orders of magnitude below the critical concentration for fibrillation in the bulk solution.

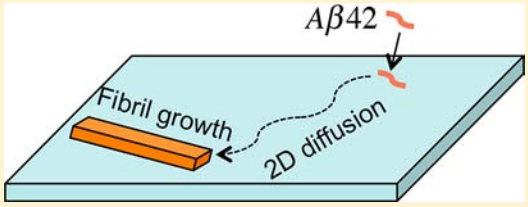

INTRODUCTION

The tendency to aggregate into amyloid fibrils is a general property of some peptides and proteins, as demonstrated in the pathogenesis of Alzheimer's, Parkinson's, and other neurodegenerative diseases.[1,2] A well-known example is the amyloid-β (Aβ42) peptide, which is predominant in neuritic plaques of Alzheimer's patients.[3] In solution, peptide and protein molecules misfold from their native conformations, assemble into oligomerized nucleus and, eventually, elongate into β-sheet filamentous aggregates. This fibril formation process involves a nucleation-dependent polymerization mechanism, in which the rate-limiting step is the formation of oligomerized nucleus characterized by a distinct lag time in growth kinetics.[4] In vitro studies in solutions have shown that fibril growth occurs only above a critical Aβ peptide concentration (17−100 μM, depending on solution conditions and peptide sequence.[4−6] This corresponds to the critical micelle concentration (CMC) in each solution.[6]

One of the most significant questions from extensive studies on fibrillation is why amyloid fibril readily forms in vivo despite the fact that the concentration of Aβ peptides in biological fluids is in the nM range,[7] which is 4 orders of magnitude lower than the CMCs in solutions.[4−6] Among the possible mechanisms proposed to explain this discrepancy, the prevalent view is that the effective local concentration of Aβ peptide can be greatly enhanced by adsorption onto molecular surfaces, particular cell membranes. In contrast to in vitro solution environments, Aβ peptides in vivo exist in a cellular environment with high concentrations of proteins, lipid membranes, and glycans. This so-called macromolecule crowding effect makes peptides in cell environment behave in radically different ways from that in test tube assays.[8] The most essential effect of macromolecule crowding is to provide a very large surface areas from cell membranes and other macromolecular surfaces. These surfaces can bind peptides and locally increase their concentrations and inter-chain interaction, thus accelerating their fibrillation. Indeed, Aβ peptides are known to interact with cell membranes, leading to membrane surface-mediated or templated assembly of Aβ fibrils.[9−14] Other in vitro studies have also demonstrated fibril formation on many different surfaces, including those of nanoparticles,[15,16] graphite,[17,18] charged mica,[19] self-assembled monolayers,[20,21] and polymeric films.[22] Molecular dynamics simulation has been exploited to study the role of liquid−solid interface on the self-organization of peptide into β-sheet fibrils.[23]

While it has been generally recognized that fibril formation in vivo may be greatly assisted or accelerated by molecular surfaces, such as cell membranes, little is known about the mechanism of surface-mediated fibrillation. Here we probe surface catalyzed fibril growth dynamics using the model system of Aβ42 on polymer surfaces with tunable hydrophobicity/hydrophilicity, as well as on supported lipid bilayer membranes. We find that Aβ42 fibrillation is inhibited on either highly hydrophilic or highly hydrophobic surfaces, but occurs readily on surfaces of intermediate hydrophobicity. The key to surface-mediated fibrillation is the presence of weakly adsorbed peptide monomers with sufficient two-dimensional mobility, as

Received: June 4, 2012
Published: August 6, 2012

dx.doi.org/10.1021/ja305398f | J. Am. Chem. Soc. 2012, 134, 14172−14178

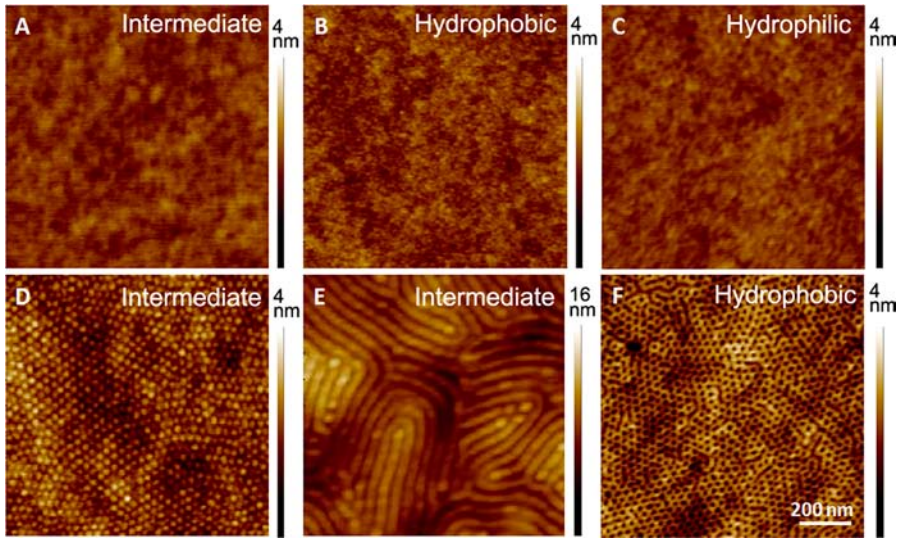

Figure 1. AFM images of thin films and corresponding hydrophobicity (in water contact angles, θ_C) of six surfaces: (A) PHEMA ($\theta_C = 55 \pm 2°$); (B) PS ($\theta_C = 102 \pm 2°$); (C) PEG ($\theta_C < 10°$); (D) PS_{60}-*b*-$PHEMA_{150}$ ($\theta_C = 62 \pm 2°$); (E) PS_{140}-*b*-$PHEMA_{150}$ ($\theta_C = 67 \pm 2°$); (F) PS_{200}-*b*-$PHEMA_{50}$ ($\theta_C = 92 \pm 2°$); The surfaces are divided into three categories: hydrophobic ($\theta_C \geq 90°$), hydrophilic ($\theta_C \leq 10°$), or intermediate ($\theta_C \approx 50-70°$). The diameters of PS domains (bright) in D or PHEMA domains (dark) in F are ~20 nm. The width of each PS (bright) or PHEMA (dark) domain in E is ~50 nm.

determined by single molecule fluorescent tracking. We show that such a mobile peptide-mediated mechanism is also responsible for fibrillation on the lipid membrane surface.

EXPERIMENTAL SECTION

Materials. Aβ42 was purchased from Sigma-Aldrich (NJ, USA) and its purity confirmed by mass spectroscopy (Figure S2 in Supporting Information). Fluorescence TAMRA-tagged Aβ42 was purchased from AnaSpec Inc. (CA, USA). Egg phophatidylcholine (EggPC) lipids were purchased from Avanti Polar lipids (AL, USA), Phosphate buffered saline (PBS) was freshly prepared from sodium and potassium salts: NaCl, KCl, Na_2HPO_4, and KH_2PO_4 to give a pH of 7.4 at 25 °C.

Aβ42 Peptide Solution. We followed the procedure of ref 18 in preparing the peptide solution. We first fully dissolved lyophilized Aβ42 in the organic solvent dimethyl sulfoxide (DMSO) at a concentration of 1 mg/mL solution. The DMSO solution was then diluted in a large amount of PBS (pH 7.4) to a final concentration of 1.0 μM. The freshly prepared Aβ42 solution (1.0 μM) was used in all experiments. Note the 1.0 μM concentration used here is not only more than 1 order of magnitude lower than the critical micelle concentrations[4−6] for Aβ42, but also a factor of 2−15 lower than the reported post-aggregation solubility[4] of Aβ42. Thus, there is no pre-aggregation or fibril growth in the aqueous solution.

Polymer Thin Film. Polystyrene-*block*-poly(2-hydroxyethyl methacrylate) (PS_{200}-*b*-$PHEMA_{50}$, molecule weight M_{PS} = 21000, M_{PHEMA} = 6300, and polydispersity index M_w/M_n = 1.10), PS_{60}-*b*-$PHEMA_{150}$ (M_{PS} = 6200, M_{PHEMA} = 20500, and M_w/M_n = 1.18), PS_{140}-*b*-$PHEMA_{150}$ (M_{PS} = 15000, M_{PHEMA} = 20500, and M_w/M_n = 1.15) diblock copolymers and polystyrene (M_{PS} = 79000, and M_w/M_n = 1.04) were obtained from Polymer Source, Inc. (Montreal, Canada) and used as received. Poly(2-hydroxyethyl methacrylate) (PHEMA) was obtained from Sigma-Aldrich (NJ, USA). All solvents used were reagent grade (Fisher). PS_{200}-*b*-$PHEMA_{50}$ (0.5 wt%) was dissolved in $CHCl_3$. PS_{60}-*b*-$PHEMA_{150}$ (1.0 wt%) and PS_{140}-*b*-$PHEMA_{150}$ (1.0 wt %) was dissolved in THF . PS (0.5 wt%) was dissolved in toluene and PHEMA (1.0 wt%) was dissolved in DMF. Each polymer thin film was spin-coated on a freshly prepared substrate (gold or glass) at 3000 rmp for 60 s. This was followed by solvent annealing in $CHCl_3$/DMF (1:1 v:v) vapor for 3 h to allow microphase separation. The PEG-coated surfaces were gifts from MicroSurfaces, Inc. (Austin, TX, USA).

Supported Lipid Bilayers. The eggPC lipids dissolved in chloroform were dried and reconstituted in an aqueous buffer (PBS, pH = 7.5) to reach a total lipid concentration of 1 mg/mL. Suspension of the lipid mixture was forced through a polycarbonate filter with 30 nm pores more than 10 times to prepare the SUV solution. To form a supported lipid bilayer, we incubated a clean glass surface in the SUV solution for ~60 min. We removed the excess vesicles from the surface by flushing the surface (under aqueous solution) for approximately 10 s with the buffer solution. The buffer solution was then exchanged with the Aβ42 peptide solution for single molecule fluorescence tracking experiments or for fibril growth. For in situ SPR probing (see Figure 5A), we used a glass-coated Au surface, as detailed in the Supporting Information. We confirmed the formation of the fluidic supported lipid bilayer using the standard method of fluorescence recovery after photo-bleaching[24] (Figure S3 in Supporting Information).

Measurements. *Atomic Force Microscopy (AFM).* The morphology of polymer thin films and the fibrils on the polymer surfaces was imaged on an AFM (Agilent Technologies 5500) in the AC mode at room temperature (25 °C). For the imaging of fibrils, we removed each surface from the Aβ42 peptide solution, rinsed it with purified water, and imaged it under ambient conditions. A silicon cantilever-mounted tip (10 nm radius of curvature, 42 N/m spring constant; 300 kHz resonance frequency) was used in all experiments.

Surface Plasmon Resonance (SPR). SPR measurements were carried out on a commercial instrument (SPRImager II, GWC Technologies Inc., Madison, WI) with the sample cell temperature at 37 °C. The surface plasmon is excited by collimated polychromatic *p*-polarized light directed at a gold film sample through a prism assembly at an angle of incidence θ. The intensity change (ΔI) measured at a constant angle is directly proportional to the change in the bulk refractive index of a solution near the sensor surface. The effective thickness (d) for the adsorbed layer is given by $d = (l_d/2)[\Delta I/s(n_a - n_s)]$, where l_d is the decay length of the evanescent field near the gold surface (typically 37% of the wavelength of the light); s is a calibrated sensitivity parameter for the instrument; n_a = 1.690 is the refractive index of adsorbent and n_s = 1.334 is the refractive index of the solution. From the effective thickness determined in the experiment, we can estimate the surface coverage (C) of adsorbed molecules as: C (molecules/cm^2) = d/V where V is the specific volume (0.738 cm^3/g for Aβ42). The dimensions of the fluidic channel and the flow rate (3 μL/s) correspond to Lamellar flow.

dx.doi.org/10.1021/ja305398f | J. Am. Chem. Soc. 2012, 134, 14172−14178

Total Internal Reflection Fluorescence Microscopy (TIRFM). TIRFM experiments were carried out at room temperature (25 °C) on a partially home-built instrument based on an inverted microscope (Nikon, TE2000). A green He−Ne laser (Melles Griot, λ_{exc} = 543 nm) was directed into an 100× objective lens (Nikon, PlanApo TIRF, NA = 1.45) with a higher angle than the critical angle and fluorescence images were acquired on an EM-CCD camera (Andor, iXon$^+$ DU-897E). The penetration depth of an evanescent wave was estimated to be ∼100 nm, and it allowed us to selectively probe blue fluorophore TAMRA-tagged Aβ42 peptides located near the glass−water interface. In each experiment, a clean cover glass coated with the particular polymer films or supported lipid bilayer was in contact with a 1 μM solution of Aβ42 containing 10^{-9} μM of TAMRA-tagged Aβ42. A series of Aβ42 fluorescence images was acquired. We obtained single molecule trajectories (positions vs time) from the time-dependent images using the ImageJ software (National Institutes of Health).

RESULTS AND DISCUSSION

We prepare surfaces of different hydrophobicity using polymer thin films, ranging from the hydrophilic poly(ethylene glycol) (PEG, $\theta_C \leq 10°$), to the intermediate poly(2-hydroxyethyl methacrylate) (PHEMA, $\theta_C = 55 \pm 2°$), and the hydrophobic polystyrene (PS, $\theta_C = 102 \pm 2°$), where θ_C is the static water contact angle. All three polymer thin films give smooth surfaces, with root-mean-square (rms) roughness less than 1 nm, as shown by atomic force microscope (AFM) images in Figure 1A−C. To prepare surfaces with intermediate hydrophobicity and to probe the possible role of compositional heterogeneity,[25−27] we use polystyrene-*block*-poly(2-hydroxyethyl methacrylate) (PS-*b*-PHEMA) diblock copolymers. The three block-copolymers thin films, PS_{60}-*b*-$PHEMA_{150}$, PS_{140}-*b*-$PHEMA_{150}$ and PS_{200}-*b*-$PHEMA_{50}$ (subscript = the number of repeating units in each block) self-organize into ordered nanoscale morphologies:[28] PS cylinder in PHEMA matrix, lying-down PS-PHEMA lamella, and PHEMA cylinder in PS matrix, respectively, as shown in AFM images (Figure 1D−F). We expect the hydrophobicity to increase with increasing PS content: PHEMA < PS_{60}-*b*-$PHEMA_{150}$ < PS_{140}-*b*-$PHEMA_{150}$ < PS_{200}-*b*-$PHEMA_{50}$ < PS. The static water contact angles for the three block-co-polymer films are $\theta_C = 62 \pm 2°$, $67 \pm 2°$, and $92 \pm 2°$, for PS_{60}-*b*-$PHEMA_{150}$, PS_{140}-*b*-$PHEMA_{150}$, and PS_{200}-*b*-$PHEMA_{50}$, respectively.

Before addressing fibril growth on the above polymer surfaces with varying hydrophobicity, we first probe the interaction of Aβ42 peptide using surface plasmon resonance (SPR) spectroscopy, Figure 2. In each experiment, we equilibrate a gold SPR sensor coated with a particular polymer thin film with PBS buffer solution in a flow cell and then switch to Aβ42 solution (1 μM in PBS) at time "a"; the delay in signal rise is the time it takes for the solution to reach the sensor surface. After a fixed time of ∼400 s, we switch the solution to PBS buffer again (time "b") to wash weakly bound peptides away and stop the adsorption process. The SPR response curves quantify the amounts of peptide molecules irreversibly (A_i) and reversibly (A_r) adsorbed on each surface. Here A_i can be simply obtained from the change in signal after the completion of the peptide exposure and washing steps, as illustrated in Figure 2 for the PS surface. To quantify A_r during the exposure of each surface to peptide solution requires the background solution signal (I_s) that results from the differences in the refractive index between the peptide solution and the buffer solution. The PEG surface is repulsive to peptide adsorption and the absence of adsorbed peptides was confirmed by the total internal reflection fluorescence (TIRF) microscopy experiments (see below). Thus, the SPR signal increase during the exposure of the PEG surface to the peptide solution is a measure of the background I_s. On each surface, the amount of reversibly adsorbed peptides is then given by: $A_r = I_t - I_s - A_i$, where I_t is the total SPR signal increase during exposure of each surface to peptide solution.

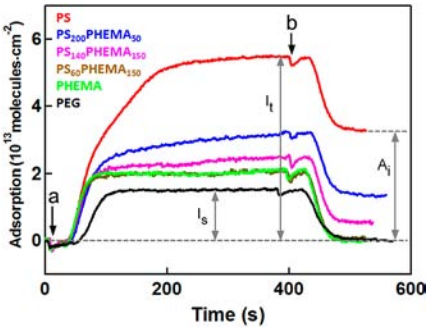

Figure 2. SPR responses for Aβ42 peptide (1 μM in PBS) adsorption on PEG, PHEMA, PS_{60}-*b*-$PHEMA_{150}$, PS_{140}-*b*-$PHEMA_{150}$, PS_{200}-*b*-$PHEMA_{50}$ and PS surfaces. The solution flow rate was ∼3 μL/s. The flow rate for the experiment on PEG was slightly lower.

Table 1 summarizes the A_i and A_r values for all the surfaces investigated. The amount of irreversibly adsorbed peptides is negligible on the hydrophilic or intermediate surfaces of PEG, PHEMA, and PS_{60}-*b*-$PHEMA_{150}$, but increases with surface hydrophobicity to (0.5 ± 0.1)-, (1.3 ± 0.2)-, and (3.2 ± 0.1) × 10^{13} molecules/cm^2 on the PS_{140}-*b*-$PHEMA_{150}$, PS_{200}-*b*-$PHEMA_{50}$, and PS surfaces, respectively. The amount of reversibly adsorbed peptides decreases slightly from (0.8 ± 0.1) × 10^{13} molecules/cm^2 on PS to (0.5 ± 0.1) × 10^{13} molecules/cm^2 on PHEMA. Both A_i and A_r are negligible on PEG.

To further establish the nature of adsorbed Aβ42 peptides, particularly their mobility on the surfaces, we carry out single molecule fluorescence tracking measurement using total internal reflection fluorescence (TIRF) microscopy. In the experiment, we record the fluorescence images of individual molecules as a function of time for each surface in contact with a 1 μM solution of Aβ42 containing 10^{-9} μM of fluorescence dye-tagged Aβ42. This 10^9 times dilution allows us to track the trajectory of single dye-tagged peptides in a sea of (10^9x more) peptide molecules on the surface. From the time-dependent fluorescence images (see sample video files in Supporting Information, including the one on PEG surface with negligible adsorbed peptides), we obtain trajectories of the positions of all of the molecules on the surface as a function of time. Note, in agreement with results from SPR spectroscopy (Table 1), we find that the total fluorescence signal of adsorbed Aβ42 peptides on PS is an order of magnitude higher than that on PHEMA. Representative single molecule trajectories on two surfaces (PS and PHEMA) are shown in Figure 3A. The Aβ42 peptide diffuses much faster on PHEMA than on PS. To quantify the diffusion coefficient constants (D) from the trajectories,[29] we plot the mean-square-displacement (MSD) against elapsed time (t) for each surface, Figure 3B$_1$,B$_2$. The linear dependence of MSD on time t indicates random Brownian diffusion D, i.e., MSD(t) = 4Dt. From the linear fits (black lines), we obtain diffusion constants (D) for 30−60 molecules in each system. Figure 3C shows histograms of diffusion constants D of Aβ42 on PS, PS_{200}-*b*-$PHEMA_{50}$, PS_{140}-*b*-$PHEMA_{150}$, and PHEMA surfaces with mean values of 0.6, 1.9, 3.3, and 26 μm^2/s, respectively. Note the logarithmic scale

dx.doi.org/10.1021/ja305398f | J. Am. Chem. Soc. 2012, 134, 14172−14178

Table 1. Amounts of Irreversibly (A_i) and Reversibly (A_r) Adsorbed Peptides from SPR Measurement, Surface Diffusion Coefficient (D) of Adsorbed Peptides from Single Molecule Fluorescence Tracking, and Static Water Contact Angles (θ_C) of the Polymer Surfaces[a]

	surface					
property	PS	PS_{200}-*b*-$PHEMA_{50}$	PS_{140}-*b*-$PHEMA_{150}$	PS_{60}-*b*-$PHEMA_{150}$	PHEMA	PEG
irrev Aβ42 ads, A_i ($\times 10^{13}$/cm^2)	3.2 ± 0.1	1.3 ± 0.1	0.5 ± 0.1	<0.1	<0.1	~0.0
rev Aβ42 ads, A_r ($\times 10^{13}$/cm^2)	0.8 ± 0.1	0.7 ± 0.1	0.5 ± 0.1	0.5 ± 0.1	0.5 ± 0.1	~0.0
H_2O contact angle (°)	102 ± 2	92 ± 2	67 ± 2	62 ± 2	55 ± 2	<10
diff constant (μm^2/s)	(0.60)	(1.9)	(3.3)		(22 ± 12)	N/A
slow	0.14 ± 0.05	0.22 ± 0.10,	0.45 ± 0.21,		N/A	N/A
fast	2.9 ± 2.1	5.6 ± 3.6	5.8 ± 4.8		22 ± 12	N/A
fibril growth	no	no	yes	yes	yes	no

[a]The diffusion constants on each surface are shown in mean values (parentheses) and in both fast and slow channels. Fibril growth is only seen (in AFM imaging) on surfaces of intermediate hydrophobicity, where reversibly adsorbed peptides accounting for half or more of adsorbed peptides.

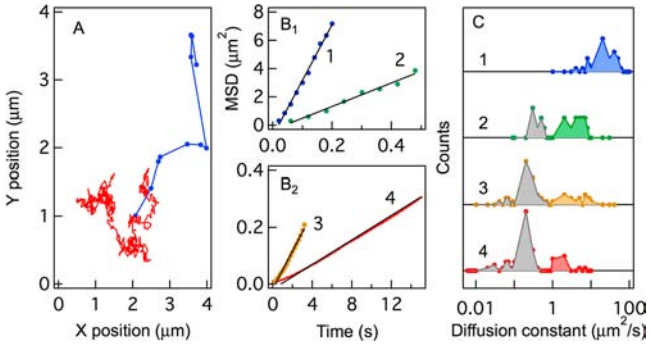

Figure 3. (A) Single molecule trajectories of Aβ42 on PHEMA (blue, 12 successive steps, 20 ms per step) and PS (red, 601 successive steps, 200 ms per step) surfaces. (B) Mean-squared displacement (MSD) as a function of time for sample single molecule trajectories of Aβ42 on (1) PHEMA, (2) PS_{140}-*b*-$PHEMA_{150}$, (3) PS_{200}-*b*-$PHEMA_{50}$, and (4) PS surfaces. Note that the data are presented on two different scales (B_1 and B_2) for clarity. Solid lines are linear fits to MSD(t) = 4Dt, where D is the two-dimensional diffusion constant. (C) Histograms of the diffusion coefficients of Aβ42 monomers on four polymer films: (1) PHEMA, (2) PS_{140}-*b*-PHEMA150, (3) PS_{200}-*b*-$PHEMA_{50}$, and (4) PS. Each diffusion constant is obtained from the MSD vs time plot of a single trajectory. Up to 60 single molecule trajectories on every surface are analyzed to give each histogram. The data sets are offset for clarity and the solid horizontal line correspond to zero counts in each case. Note the logarithmic scale for the X-axis. The scale-bar (5 counts) for the Y-axis is shown. The color-hatched areas indicate the weakly adsorbed and highly mobile population and the gray-hatched areas represent the strongly adsorbed and slowly diffusing population.

for the X-axis. On PS, PS_{200}-*b*-$PHEMA_{50}$, and PS_{140}-*b*-$PHEMA_{150}$ surfaces, the histogram on each surface is clearly bimodal, with a slower and more narrowly distributed component ($D \approx 0.1-0.5$ μm^2/s, gray-hatched areas) and a faster and more broadly distributed component ($D \approx 1-10$ μm^2/s, color-hatched areas). The presence of these two channels is in agreement with the two types of adsorbed peptides, irreversible and reversible, as determined in SPR measurements (Table 1). The relative population of the slow channel increases with increasing surface hydrophobicity or surface PS composition, in excellent agreement with the increasing surface coverage of irreversibly adsorbed peptides. Thus, we assign the slowly diffusing component to irreversibly adsorbed peptides and the fast one to reversibly adsorbed peptides. On the PHEMA surface, the histogram is characterized by only a fast component (D = 22 ± 12 μm^2/s), as expected from the absence of irreversibly adsorbed peptides determined by SPR (Table 1).

The SPR and TIRF results can be summarized as follows. PEG is the only surface repulsive to Aβ42 peptides adsorption. On all other surfaces, there are weakly and reversibly adsorbed peptides (Table 1) that possess sufficient two-dimensional mobility (D = 2.9–22 μm^2/s). In addition to the mobile and weakly adsorbed species, there are also strongly and irreversibly adsorbed Aβ42 peptides with low diffusion constants (0.14–0.45 μm^2/s) on surfaces containing ~50% or more of the hydrophobic PS. The amount of irreversibly adsorbed Aβ42 peptides increases with increasing surface hydrophobicity (PS_{140}-*b*-$PHEMA_{150}$ < PS_{200}-*b*-$PHEMA_{50}$ < PS). While the distributions of diffusion constants for both reversibly adsorbed (color-hatched areas in Figure 3C) and irreversibly adsorbed (gray-hatched areas in Figure 3C) are broad, we see a qualitative anti-correlation between the diffusion constants and surface hydrophobicity, in agreement with known properties of weakly adsorbed protein and polymer molecules at solid–liquid interfaces.[30,31]

We now probe the growth of Aβ42 amyloid fibril on these model polymer surfaces at a temperature of 37 °C and in a solution Aβ42 concentration of 1 μM (in PBS). Any fibril observed must be formed at the solid–liquid interfaces as this peptide concentration is more than 1 order of magnitude lower than the critical concentration for fibril formation in the solution phase.[4−6] After incubation for 18 h, the polymer surfaces are rinsed with plenty of pure water and then characterized by AFM, Figure 4. Long and relatively straight Aβ42 fibrils readily grow on the PHEMA surface (Figure 4A), but to a lesser extent on the more hydrophobic PS_{60}-*b*-$PHEMA_{150}$ (Figure 4D) and PS_{140}-*b*-$PHEMA_{150}$ (Figure 4E) surfaces. There is no fibril formation on the most hydrophobic PS surface (Figure 4B), but only islands of strongly adsorbed peptide molecules, inter-dispersed with spots of bare PS surfaces. On PS_{200}-*b*-$PHEMA_{50}$ surface (Figure 4F) with the hydrophobic PS domain as majority matrix, we observe short Aβ42 aggregates, not elongated fibrils, in agreement with a recent study on the influence of hydrophobicity on surface-catalyzed amyloid fibril formation.[32] As expected, the hydrophilic and repulsive PEG surface remains clean and there is no fibril growth or peptide adsorption (Figure 4C). We can clearly resolve the helical internal structure[33] of the fibril in AFM images; this is most obvious for the long and straight fibrils on the PHEMA surface (inset in A). The AFM images taken after different peptide incubation time also allow us to quantify fibril growth kinetics (see Figure S1 in Supporting Information),

dx.doi.org/10.1021/ja305398f | J. Am. Chem. Soc. 2012, 134, 14172–14178

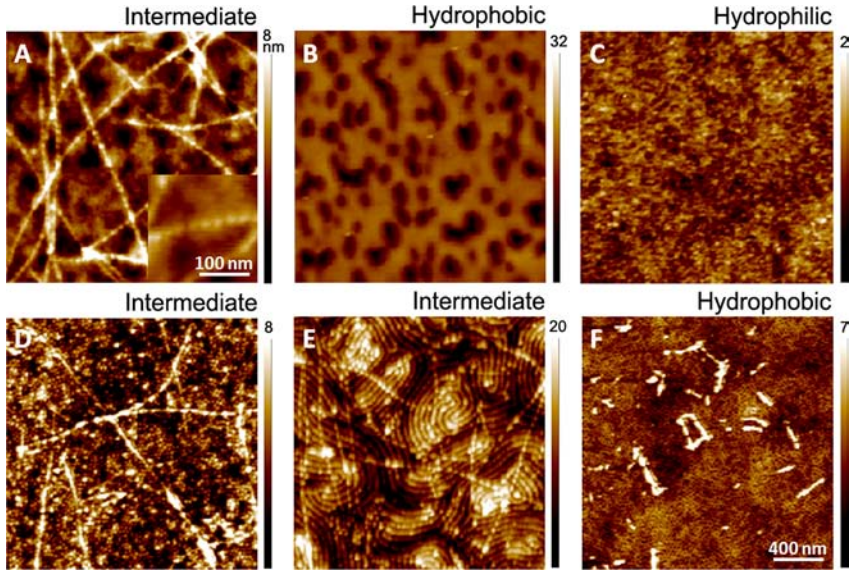

Figure 4. AFM images taken in the air for the polymer this films thin films (see Figure 1) after they have been incubated in Aβ42 peptide solution (1 μM in PBS) at 37 °C for 18 h: (A) PHEMA, (B) PS, (C) PEG, (D) PS_{60}-*b*-$PHEMA_{150}$, (E) PS_{140}-*b*-$PHEMA_{150}$, and (F) PS_{200}-*b*-$PHEMA_{50}$. The inset in panel A is a zoomed-in image showing the helical structure of the fibril. The width of each fibril is ~20 nm. The scale bar is 400 nm (for all panels). The pseudo color scales (height) are in units of nm. The relative hydrophobicity is labeled at the top right corner of each image: hydrophobic ($\theta_C > 90°$), hydrophilic ($\theta_C < 10°$), or intermediate ($\theta_C \approx 50–70°$).

which is characterized by a known lag-time, followed by nearly linear growth.[4,34]

The growth of fibril on the surface requires the presence of weakly adsorbed and mobile peptide molecules, and is anti-correlated with the amount of irreversibly adsorbed peptides. On the PHEMA surface where there is sufficient concentration of weakly adsorbed peptides that have the highest two-dimensional diffusion coefficient ($D = 22 \pm 12$ $\mu m^2/s$), we observe the most extensive growth and the longest fibrils. The extent of fibril growth decreases with decreasing peptide mobility or increasing amount of irreversibly adsorbed peptides on PS_{60}-*b*-$PHEMA_{150}$ and PS_{140}-*b*-$PHEMA_{150}$ and ceases when more slowly moving and irreversibly adsorbed peptides dominate on PS_{200}-*b*-$PHEMA_{50}$ or PS. On the PEG surface, there are no adsorbed peptides and no fibril growth. We conclude that the growth of amyloid Aβ42 fibril at the solid–liquid interfaces requires the dominance of weakly adsorbed peptides with sufficient two-dimensional mobility on the surface. The alternative mechanism is which peptide molecules in the solution phase directly add to the end of a growing fibril on the surface can be ruled out, as such a mechanism should not be sensitive to surface physical properties, including hydrophobicity/hydrophilicity or surface diffusion constant. Note that compositional surface heterogeneity on the nanometer scale is known to affect protein adsorption,[25−27] but it seems to have little effect on fibrillation: for the homogeneous PHEMA surface and the heterogeneous PS_{60}-*b*-$PHEMA_{150}$ and PS_{140}-*b*-$PHEMA_{150}$ surfaces, we find the extent of fibril growth is only correlated with the relative population of the mobile fraction of adsorbed peptides.

Cell membrane surfaces are believed to be important in catalyzing fibril formation in vivo. In fact, freely diffusing peptides on the cell membrane surface has been proposed to be responsible for helical aggregated formation, leading to membrane-mediated fibrillation.[35] In view of the present findings on model polymer surfaces, we may ask the following critical question: *Is the surface-mediated mobile precursor mechanism relevant to fibril growth in vivo?*

While providing a direct answer to this question is difficult, we carry out an in vitro experiment on supported lipid bilayer (SLB) membranes. We form supported lipid bilayers on glass surfaces using well-established method of vesicle fusion.[36] This SLB formation process can be directly followed in situ by SPR as we expose a glass-coated Au surface to a solution of small unilamellar vesicles (SUVs) of egg phophatidylcholine (EggPC), red curve in Figure 5A. After SUV incubation and buffer washing, we observe an irreversible increase in SPR intensity, corresponding to an SLB thickness of 4.5 ± 0.5 nm, as expected for a lipid bilayer. SPR measurement (blue curve in Figure 5A) shows the absence of irreversible peptide adsorption on the SLB surface, as shown by the negligible change in SPR intensity before peptide injection and after buffer wash. The most inportant result comes from single molecule fluorescence tracking (see sample video file in Supporting Information). Figure 5B shows a histogram of two-dimensional diffusion constants (D) of Aβ42 on the SLB surface, with a sample single molecule trajectory shown in the inset. Compared the histograms on model polymer surfaces in Figure 3C, the histogram of peptide diffusion constants on the lipid membrane surface (mean diffusion constant $\langle D \rangle = 23$ $\mu m^2/s$) is similar to, but slightly broader than, that on the most mobile PHEMA surface. Based on results from model polymer surfaces, we expect that Aβ42 fibrils should grow from the mobile peptides on the lipid membrane surface, as confirmed by AFM imaging, Figure 5C. It is known from extensive studies in the past on lipid membranes that fibrillation may be enhanced by surface chemical properties, such as charge status of lipid head groups, the incorporation of cholesterol, and the presence of glycol groups (e.g., gangliosides).[10−14] In view of the presence of mobile peptide precursors also on the membrane surface, we believe such enhancement in fibrillation come from an increase in mobile peptide populations or the promotion of inter-peptide interaction on the membrane surface.

dx.doi.org/10.1021/ja305398f | *J. Am. Chem. Soc.* 2012, 134, 14172−14178

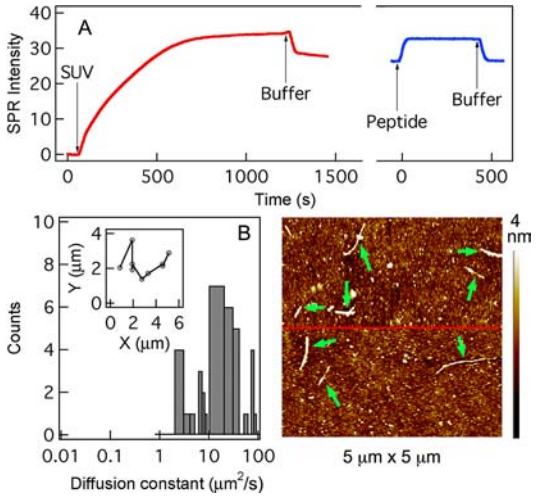

Figure 5. (A) SPR response of the formation of supported lipid bilayer (SLB, red) on SiO_2-coated gold substrate and the subsequent adsorption of Aβ42 peptide (blue) on SLB. The arrows indicate the times for the injection of small unilamellar vesicle (SUV) solution, buffer solution, and peptide solution (1 μM in PBS buffer), respectively. (B) Histogram of the diffusion coefficients of Aβ42 monomers ($\langle D \rangle$ = 23 $\mu m^2/s$) on the SLB surface, obtained from single molecule fluorescence tracking (see Supporting Information for a video). The inset shows a typical single molecule trajectory surface (9 successive steps, 100 ms per step) of Aβ42 on the SLB surface. (C) AFM image of SLB surface after it has been incubated in Aβ42 peptide solution (1 μM in PBS) at 37 °C for 18 h. The 5 μm × 5 μm image consists two scans (separated by the red line). The green arrows point to features attributed to fibrils.

CONCLUSIONS

The discoveries presented here show how a surface can facilitate fibrillation: the surface serves to locally concentrate peptide molecules and the confinement of the two-dimensional environment promotes inter-peptide interaction, leading to fibrillation at Aβ peptide concentration many orders of magnitude below the critical concentration for fibrillation in the bulk solution (biological fluids). Surface physical properties that can increase the concentrations of weakly adsorbed peptides while maintaining sufficient translational mobility on the surface can promote fibrillation. Sufficient mobility is critical as it allows precursor peptides within the two-dimensional "reservoir" to diffuse along the surface and attach onto the ends of a growing fibril. Any process disrupting the formation or mobility of these mobile precursors will disrupt fibril growth, as is the case on the PS, PS_{200}-*b*-$PHEMA_{50}$, or PEG surface. On the PS or PS_{200}-*b*-$PHEMA_{50}$ surface, strong surface/peptide attraction leads to irreversibly adsorbed peptides with low two-dimensional diffusion constants (0.1−0.5 $\mu m^2/s$), thus inhibiting fibril growth. On PEG, the surface is too respulsive for peptide adsorption and thus prohibits fibril formation. A balance between transient concentration and mobility of the peptide precursor is best exemplified by the PHEMA polymer surface where adsorbed peptides are highly mobile and fibril formation readily occurs. This principle also applies to biological environments, e.g., fibrillation on cell membranes. Properties that promote the adsorption of weakly bound peptides, such as particular charge groups or the presence of cholesterol and lipid drafts, can promote fibrillation.[9−14] In many ways, fibrillation can be viewed as the growth of a one-dimensional crystal and the necessity of mobilie precursor states in crystal growth is a well-established concept in the field of crytalline thin-film growth in materials science.[37]

ASSOCIATED CONTENT

Supporting Information

Results from control experiments and complete author lists for some references. Time-dependent fluorescence images showing two-dimensional movement of fluorescent-tagged peptide on six surfaces (si_002.avi = PEG.avi; si_003.avi = SupportedLipidBilayer.avi; si_004.avi = PHEMA.avi; si_005.avi = PS140PHEMA150.avi; si_006.avi = PS200PHEMA50.avi; si_007.avi = PS.avi). This material is available free of charge via the Internet at http://pubs.acs.org.

AUTHOR INFORMATION

Corresponding Author

zhu@cm.utexas.edu

Notes

The authors declare no competing financial interest.

ACKNOWLEDGMENTS

This work was supported by the U.S. Army Research Office grant W911NF-08-1-0287 and the University of Texas at Austin. We thank Dr. Jan Vogelsang and Ms. Katherine Koen for helpful discussions on TIRF microscopy and single molecule tracking.

REFERENCES

(1) Dobson, C. M. *Nature* **2003**, *426*, 884.
(2) Soto, C. *Nat. Rev. Neurosci.* **2003**, *4*, 49.
(3) Hamley, I. W. *Angew. Chem., Int. Ed.* **2007**, *46*, 8128.
(4) Harper, J. D.; Lansbury, P. T., Jr *Anuu. Rev. Biochem.* **1997**, *66*, 385−407.
(5) Lomakin, A.; Chung, D. S.; Benedek, G. B.; Kirschner, D. A.; Teplow, D. B. *Proc. Natl. Acad. Sci. U.S.A.* **1996**, *93*, 1125.
(6) Sabate, R.; Estelrich. *J. Phys. Chem. B* **2005**, *109*, 11027.
(7) Seubert, P.; et al. *Nature* **1992**, *359*, 325.
(8) Ellis, R. J. *Trends Biochem. Sci.* **2010**, *26*, 597.
(9) Terzi, E.; Holzemann, G.; Seelig, J. *Biochemistry* **1997**, *36*, 14845.
(10) Tip, C. M.; Darabie, A. A.; McLaurin, J. *J. Mol. Biol.* **2002**, *318*, 97.
(11) Jayasinghe, S. A.; Langen, R. *Biochemistry* **2005**, *44*, 12113.
(12) Matsuzaki, K. *Biochem. Biophys. Acta* **2007**, *1768*, 1935.
(13) Chi, E. Y.; Ege, C.; Winans, A.; Majewski, J.; Wu, G.; Kjaer, K.; Lee, K. Y. C. *Proteins* **2008**, *72*, 1.
(14) Hebda, J.; Miranker, A. D. *Annu. Rev. Biophys.* **2009**, *38*, 125.
(15) Linse, S.; et al. *Proc. Natl. Acad. Sci. U.S.A.* **2007**, *104*, 8691.
(16) Pronchik, J.; He, X.; Giurleo, J. T.; Talaga, D. S. *J. Am. Chem. Soc.* **2010**, *132*, 9797.
(17) Brown, C.; Aksay, I. A.; Saville, D. A.; Hecht, M. H. *J. Am. Chem. Soc.* **2002**, *124*, 6846.
(18) Kowalewski, T.; Holtzman, D. M. *Proc. Natl. Acad. Sci. U.S.A.* **1999**, *96*, 3688.
(19) Zhu, M.; Souillac, P. O.; Ionescu-Zanetti, C.; Carter, S. A.; Fink, A. L. *J. Biol. Chem.* **2002**, *277*, 50914.
(20) McMasters, M. J.; Hammer, R. P.; McCarley, R. L. *Langmuir* **2005**, *21*, 4464.
(21) Ku, S. H.; Park, C. B. *Langmuir* **2008**, *24*, 13822.
(22) Nayak, A.; Dutta, A. K.; Belfort, G. *Biochem. Biophys. Res. Commun.* **2008**, *369*, 303.
(23) Nikolic, A.; Baud, S.; Rauscher, S.; Pomes, R. *Proteins* **2011**, *79*, 1.
(24) Deng, Y.; et al. *J. Am. Chem. Soc.* **2008**, *130*, 6267.
(25) Vörös, J.; Blättler, T.; Textor, M. *MRS Bull.* **2005**, *30*, 202.

(26) Baxamusa, S. H.; Gleason, K. K. *Adv. Funct. Mater.* **2009**, *19*, 3489.
(27) Miller, R.; Guo, Z.; Vogler, E. A.; Siedlecki, C. A. *Biomaterials* **2006**, *27*, 208.
(28) Bates, F. S.; Fredrickson, G. H. *Annu. Rev. Phys. Chem.* **1990**, *41*, 525.
(29) Anthony, S.; Zhang, L.; Granick, S. *Langmuir* **2006**, *22*, 5266.
(30) Tilton, R. D. *Surf. Sci. Ser. : Biopolym. Interf.* **1998**, *75*, 363.
(31) Sukhishvili, S. A.; Chen, Y.; Müller, J. D.; Gratton, E.; Schweizer, K. S.; Granick, S. *Nature* **2000**, *406*, 146.
(32) Keller, A.; et al. *ACS Nano* **2011**, *5*, 2770.
(33) Roher, A. E.; et al. *J. Biol. Chem.* **1996**, *271*, 20631.
(34) Jarrett, J. T.; Lansbury, P. T., Jr *Cell* **1993**, *73*, 1055.
(35) Knight, J. D.; Hebda, J. A.; Miranker, A. D. *Biochemistry* **2006**, *45*, 9496.
(36) Brian, A. A.; McConnell, H. M. *Proc. Natl. Acad. Sci. U.S.A* **1984**, *81*, 6159.
(37) Tsao, J. Y. *Materials Fundamentals of Molecular Beam Epitaxy*; Academic Press: San Diego, 1993.